ARTICLE

Two [Ln_4] molecular rings folded as compact tetrahedra

Jorge Salinas-Uber,[a] Leoní A. Barrios,[a,b] Olivier Roubeau,[c] and Guillem Aromí [a,b,*]

Received 00th January 20xx,
Accepted 00th January 20xx

DOI: 10.1039/x0xx00000x

The design of photoactive ligands may provide an entry into multifunctional molecular nanomagnets. We report here the design and synthesis of a new multitopic chelating ligand, 1,2-bis-(5-(N'-(pyridine-2-yl-methylene)-carbohydrazide)-3-methyl-thien-3-yl)-cyclopentene (H_2L), bearing a photoswitchable spacer and demonstrate that it undergoes reversible photo isomerization in solution. In the presence of the base NaH, H_2L reacts with $LnCl_3$ salts (Ln=Dy, Tb) to form the supramolecular assemblies $H_2O@[Ln_4L_4Cl_4(H_2O)_4]$ (Ln=Dy, **1**; Tb, **2**). Single crystal X-ray diffraction data from **1** and **2** reveal that both compounds consist of highly symmetric molecular rings efficiently folded through intramolecular weak interactions in form of tetrahedra. This arrangement imparts a conformation onto the photochromic spacer of the ligand that inhibits its photoswitching activity. Despite the low symetry of the coordination geometry around the Ln ions, the Dy analog exhibits slow relaxation of the magnetization. The relaxation rate under various conditions has been investigated, allowing to elucidate the mechanisms operating for this relaxation.

Introduction

Lanthanide coordination chemistry is of relevance to a large number of scientific areas and applications ranging light-emitting diodes,[1] molecular information storage,[2-5] magnetic refrigeration,[6-8] magnetic resonance imaging[9] or quantum computing.[10-15] On the topic of molecular magnetism, a Dy(III) organometallic complex has emerged as an outstanding single molecule magnet (SMM), with a record blocking temperature above liquid nitrogen.[16] Indeed, compounds of this metal are known to exhibit very often slow relaxation of the molecular magnetic moment.[3, 17] Dy(III) is therefore, an excellent ingredient in the search of magnetic molecular materials capable of switching or modulating their properties reversibly by an external stimulus, such as light irradiation.[18] In the attempt to obtain molecular assemblies made of Dy(III) single ion magnets, with photo-switchable properties, we have designed and prepared a new bridging ligand, 1,2-bis-(5-(N'-(pyridine-2-yl-methylene)-carbohydrazide)-3-methyl-thien-3-yl)-cyclopentene (H_2L), incorporating a dithienylethene spacer, which undergoes a reversible light-triggered process of cyclization (Fig. 1).[19] The latter is a highly convenient photochromic unit because of its resistance to fatigue and the fact that both isomers are thermally stable. Also, because the switching takes place with a different light frequency (UV or visible) for each direction.[20] Dithienylethenes have been exploited before to design molecular species with photoswitchable magnetic properties.[21-25] Here, we have explored the reactivity of deprotonated H_2L with Dy(III) or Tb(III) chloride in an attempt to prepare Ln-based SMMs, with tuneable properties *via* photo switching processes.[26] The coordination metallocycles $H_2O@[Ln_4L_4Cl_4(H_2O)_4]$ (Ln=Dy, **1**; Tb, **2**) were obtained, highly folded to yield a compact structure with the metals disposed at the vertices of a tetrahedron. The magnetic slow relaxation properties of **1** and **2** have been studied, and the photochromic properties of all the new compounds have been explored.

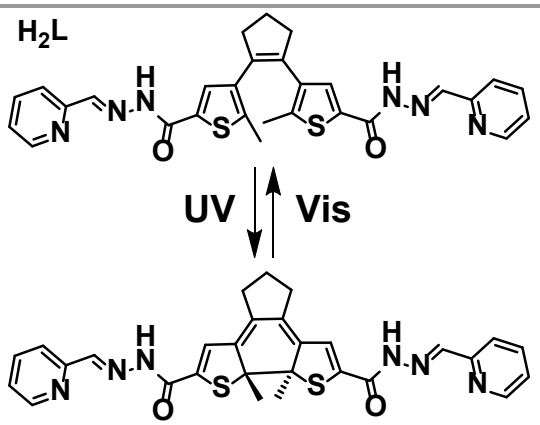

Figure 1. Ligand H_2L and the reversible photoconversion of its central dithienylpentene moiety upon UV and Visible irradiation, respectively.

Results and Discussion

Synthesis and Properties of H_2L

[a] *Departament de Química Inorgànica i Orgànica, Universitat de Barcelona, Diagonal 645, 08028 Barcelona, Spain. E-mail: guillem.aromi@qi.ub.es.*
[b] *Institut of Nanoscience and Nanotechnology of the University of Barcelona (IN2UB), Barcelona, Spain.*
[c] *Instituto de Ciencia de Materiales de Aragón (ICMA), CSIC and Universidad de Zaragoza, Plaza San Francisco s/n, 50009, Zaragoza, Spain*

† Footnotes relating to the title and/or authors should appear here.
Electronic Supplementary Information (ESI) available: [details of any supplementary information available should be included here]. See DOI: 10.1039/x0xx00000x

The ligand H_2L is synthesized by a Schiff base reaction between a bis-carbohydrazide containing a dithienylethene a spacer (1,2-bis-(5-carbohydrazide-2-methyl-thiophen-3-yl)-cyclopentene) and 2-pyridinaldehyde (Scheme S1). The analogous ligand made with salicylaldehyde (instead of pyridinaldehyde) together its reactivity with Cu(II) was recently reported.[27] this yielded coordination complexes exhibiting reversible photochromic activity. Ligand H_2L was fully characterized (see below) and its photo-switching properties in solution were studied in ethanol. Thus, irradiation of a colorless solution of H_2L with UV light causes a color change to deep violet that is completely reversed upon illumination with visible light. This photochromic behavior was monitored through electronic spectroscopy (Fig. 2). The spectrum of H_2L is dominated by an intense band at 308 nm, featuring a small shoulder at higher energies. Smaller bands at 208 and 396 nm, respectively are also present. UV irradiation causes a drastic decrease of absorbance of the 308 nm band together with the fast growth of a very broad and intense band at 564 nm, characteristic of the conjugated system formed upon photocyclization (Fig. 1), which gives the strong coloration to the closed form of the photoactive moiety.[28] A photo-stationary state (PPS) is reached in 70 seconds. The reverse process caused by visible light also occurs very fast, leading to the restoration of the original spectrum at the PPS in about 80 seconds (Fig. 2). Small differences with respect to the initial system may have to do with the potential interference by cis/trans isomerization processes of the hydrazone, susceptible to occur under light irradiation.[29]

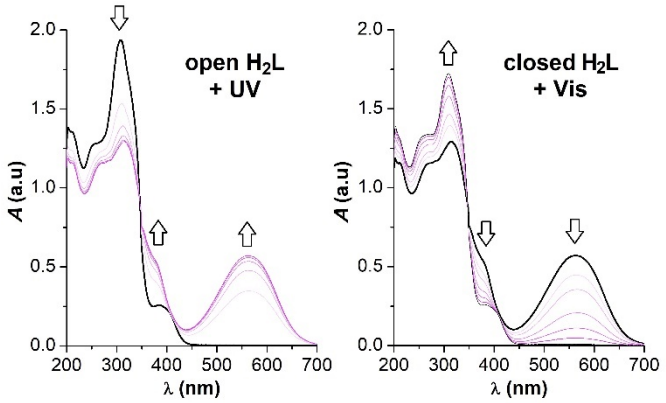

Figure 2. Absorption spectrum of 5+10^{-5} M H_2L in EtOH solution and its evolution upon irradiation first with UV light (< 425 nm, left panel) and then with visible light (> 430 nm, right panel). The initial spectrum before each series is the black thick trace.

Structures of $H_2O@[Ln_4L_4Cl_4(H_2O)_4]$ (Ln=Dy, 1; Tb, 2).

Compounds **1** and **2** are prepared through stoichiometric reactions in pyridine between H_2L and the corresponding $LnCl_3$ hydrate (Ln=Dy, Tb), using NaH to deprotonate the ligand, according to the reaction in equation 1.

$$4\ H_2L + 4\ LnCl_3 + 8\ NaH + 5\ H_2O \rightarrow$$
$$\rightarrow H_2O@[Ln_4L_4Cl_4(H_2O)_4] + 8\ NaCl + 8\ H_2 \qquad (1)$$

Both compounds are obtained as crystals, featuring quasi isostructural lattices in the tetragonal space group, $I4_1/a$ (Table S1). The asymmetric unit is composed by one Ln(III) ion, one deprotonated ligand L^{2-}, one terminal Cl^-, one coordinated molecule of H_2O, one fourth of another molecule of H_2O and, four/three lattice pyridine molecules (for **1**/**2**). Compound **2** additionally, includes half molecule of MeOH in this unit. The coordination complex (Fig. 3) is formed by four Ln(III) ions, each chelated by two (O,N,N) coordination pockets of two L^{2-} ligands, which, in this manner bridge them to two other metals of the tetranuclear cluster. Eight coordination around each lanthanide ion is completed by one Cl^- and one H_2O terminal ligand, in mutual *cis* configuration, and mutually disordered.

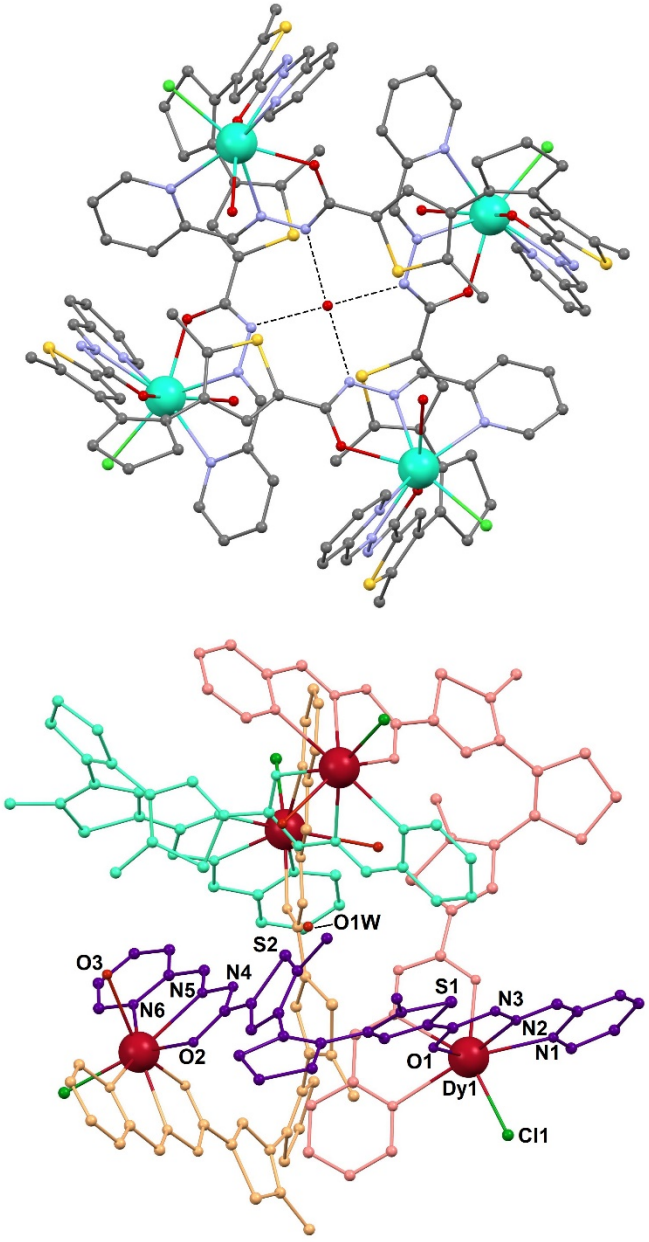

Figure 3. (top) Molecular structure of $H_2O@[Dy_4L_4Cl_4(H_2O)_4]$ (**1**) down the crystallographic *c* axis. Dy, turquoise; N, purple, O, red; C, grey; Cl, green. H atoms omitted and hydrogen bonds are shown as dashed lines. (bottom) Different view of **1** with heteroatoms of the asymmetric unit labelled and with ligands in four different colours to emphasize their conformation and coordination modes. The Cl and water terminal ligands are mutually disordered and only the main component is shown. The main molecule of complex $H_2O@[Tb_4L_4Cl_4(H_2O)_4]$ (**2**) is completely analogous.

The coordination bond distances are listed in Table S2. Thus, the aggregate consists of a [Ln_4L_4] molecular ring, which is, by virtue of the large flexibility of the ligands, highly folded onto itself. The result is a compact structure, featuring the four metals at the vertices of a flattened tetrahedron (Fig. 3, S2 and S3), with two long edges, 10.726/10.784 Å, and four shorter ones, 9.613/9.645 Å (in the **1**/**2** format). For each ligand in this structure, one hydrazone and its adjacent thienyl ring point towards the interior of the cage and the other analogous group is oriented outwards (Fig. 3). A molecule of water is allocated the centre of the assembly, establishing hydrogen bonds to the non-coordinated N-atoms of the internal hydrazone moieties, clearly contributing to the stability of the folded structure (Table S3). Static or dynamic disorder cause a symmetric relationship with each of the four N–atoms, possible acceptors of the two hydrogen bonds per molecule (O···N distance of 2.906/2.887 Å). Reinforcing the compact structure, each ligand establishes one set of intramolecular C–H···π interactions through the methyl group of one thienyl ring with its other thienyl ring and the pyridyl of an adjacent ligand (Fig. S4).

The solid-state configuration of the H_2O@[$Ln_4L_4Cl_4(H_2O)_4$] units causes the methylthiophenyl groups within each L^{2-} ligand to adopt the so-called "parallel" conformation, *i.e.* with both methyl groups oriented towards the same side of the idealized plane of the photochromic unit. This prevents the photocyclization process upon UV light irradiation,[30] as verified experimentally here.

Each molecule of **1** or **2** is surrounded in the lattice by four first neighbours interacting *via* S···S contacts (with distances of 3.401/3.397 Å), organizing the clusters in sheets perpendicular to the crystallographic *c* axis (Fig. S5).

Coordination clusters of four Ln ions in form of a tetrahedron are quite common. One category is that of compact cages with monoatomic bridges between the metals,[31-33] sometimes incorporating a central μ_4–O^{2-} ion linking all of them.[34-37] Another type is made by coordination assemblies ensembled by extended polytopic ligands spanning either the vertices[38-41] or the faces[42-46] of the tetrahedron. In this latter category, the metals at kept much further apart, therefore the cages feature large cavities, with the capacity to host various types of guests,[47-50] including molecules of water.[51] Interestingly, none of the tetrahedric [Ln_4] cages reported to the Cambridge Structure Data Center (CCDC) consist of a molecular ring assembled by ditopic ligands, folded into itself as a tetrahedron *via* intramolecular weak contacts as in **1** and **2**.

Magnetic Properties

As mentioned in the introduction, lanthanide complexes have acquired increased relevance in the area of molecular magnetism. In relation to compounds **1** and **2**, Dy(III) and Tb(III) have become part of some of the most outstanding SMMs known in the literature.[16, 52] The variable temperature molar magnetic susceptibility (χ) response of both clusters was evaluated under a constant magnetic field of 0.1/0.3 T (in the **1**/**2** format; Fig. S6). Both compounds exhibit at 300 K values of the $\chi_M T$ product (55.04/44.61 cm^3Kmol^{-1}) that are very close to these expected for four isolated Dy/Tb ions in the absence of exchange interactions (*i.e.* 56.7/47.2 cm^3Kmol^{-1} for [Dy_4]/[Tb_4] corresponding to $^6H_{15/2}/^7F_6$ terms with L = 5/3, S = $\frac{5}{2}$/3, J = $\frac{15}{2}$/6 and g = $\frac{4}{3}/\frac{3}{2}$). For both compounds, χT declines upon decreasing the temperature, with increasing rates as the latter approaches 2 K, where χT reaches 46.56/27.10 cm^3Kmol^{-1}. The decrease of the χT product with cooling is caused by depopulation of Stark levels and is more significant in **2**. Most of the decrease of χT below 10 K is however an effect of the applied *dc* field, since the equilibrium susceptibility derived from zero-field *ac* measurements reflects a much-reduced decline of χT below that temperature (Fig. S6). Besides indicating the absence of any significant exchange interaction, this observation points at the presence of slow dynamics of the magnetization, which was further investigated through *ac* susceptibility measurements. A significant out-of-phase component of the susceptibility (χ'') is indeed detected at 2 K and zero *dc* field for the [Dy_4] cluster, which is frequency dependent. However, a maximum in χ'' *vs*. frequency, which defines the characteristic relaxation time, could not be observed. The application of even small *dc* fields is nevertheless enough to bring the frequency of this maximum to within the experimental window (Figs. S7-S8, see below). This was not the case for the [Tb_4] complex, for which no χ'' signal could be detected at zero *dc* field (as measured up to ≈1kHz), while the application a *dc* magnetic field up to 0.2 T was not sufficient to have a maximum of χ'' emerge in variable-temperature measurements down to 2 K (Fig. S7). Thus, only the slow relaxation of the magnetization of the Dy complex was studied in more detail. Variable frequency (0.1 to 10 kHz) isothermal measurements on **1** were first performed at increasing applied *dc* fields at 2 K, and the characteristic relaxation times τ was extracted with the generalized Debye model (see SI, Fig. S8). τ is found to rapidly increase at low fields and already reaches *ca.* 1.5 ms at 750 Oe (Fig. 5). In the low field range studied, up to 0.1 T, the increase of τ is $\approx aB^2$, considering the estimated error, which becomes very large as soon as frequency maximum is localized closer to the limit or out of the experimental frequency window. This field-dependence, depicted in Fig. 5 also as a log-log plot, is expected for a relaxation mechanism based on the spin-spin and spin-nuclei coupling. It is also consistent with the fact that the direct process of relaxation is not yet significant at these low fields. The temperature dependence of τ was then studied at 400 and 750 Oe, as well as in zero-field (Figs. S9-11). In zero-field, the relaxation time remains approximately constant at 1-2 10^{-6} s, in agreement with a fast tunnelling relaxation. Application of a *dc* field cancels out this fast relaxation process as observed, at least at sufficiently low temperatures. Thermal activation is clearly present already above 5 K, especially at 750 Oe. At these relatively low temperatures, this is more likely due to Raman spin-phonon processes than to the Orbach mechanism, as discussed elsewhere.[53-55] The thermal dependence of τ is in fact well reproduced at both fields by the sum of both, direct and Raman relaxation processes through the expression $\tau^{-1} = aT + cT^n$, best fitted for a = 1281(69) / 53(fixed), c = 49(12) / 0.024(3) s^{-1} K^{-n} and n = 2.7(2) / 5.5(1) in the 400/750 Oe format.

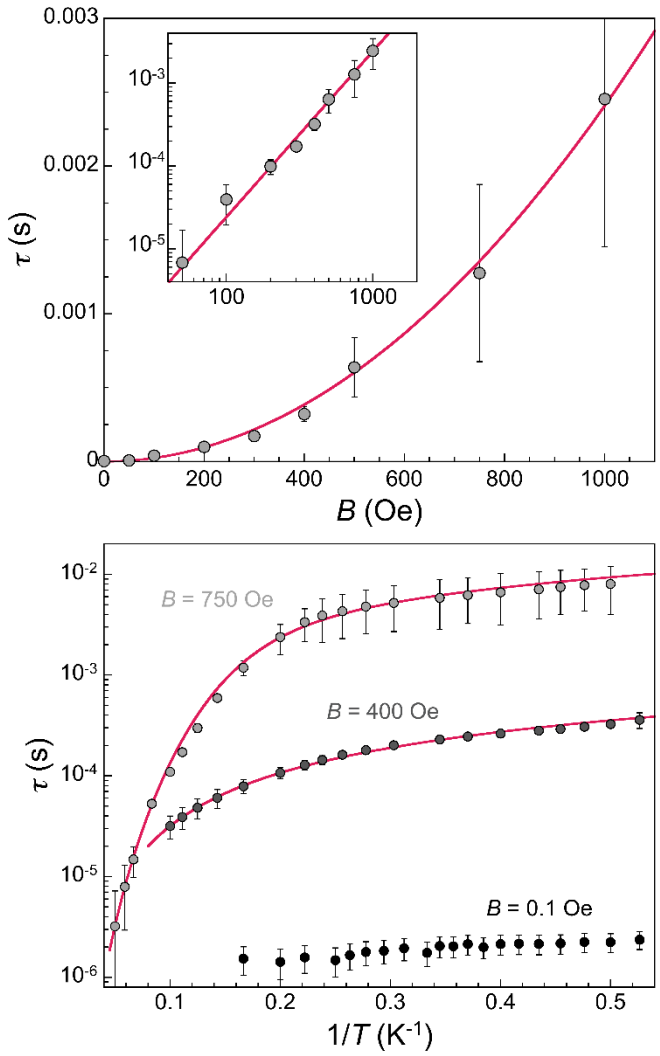

Figure 4. Relaxation time τ for **1** as a function of the *dc* magnetic field *B* at 2 K (top, inset shows a log-log plot) and of temperature at zero-field and 400 and 750 Oe applied fields (bottom). Red lines are respectively B^2 dependences (top) and a fit of the data to $\tau^{-1} = aB^2T + cT^n$ (bottom, see text).

The fast relaxation properties depicted here are understandable considering the absence of adequate local symmetry at the Dy centers in the structure of **1**, in particular, of the strong axiality necessary for SMMs with exceptionally large energy barriers to relaxation.[5, 16, 56]

While H_2L facilitates the assembly of clusters with slow relaxation of the magnetization, the metals promote a supramolecular arrangement locking effectively its photochromic activity. Future efforts will be directed at including co-ligands to the reaction mixture to isolate open assemblies. Avoiding the folding of the structure should prevent the inhibition of the photoswitching behaviour of the dithyenylethene moieties.

Experimental

Synthesis

All chemicals were purchased from Aldrich and used without further purification. All coordination chemistry reactions were performed under aerobic conditions. The precursor 1,2-bis-(5-carbohydrazide-2-methyl-thiophen-3-yl)-cyclopentene was synthesized according to a previously reported procedure.[27]

1,2-bis-(5-(N'-(pyridine-2-yl-methylene)-carbohydrazide)-3-methyl-thien-3-yl)-cyclopentene (H_2L). Solid 1,2-bis-(5-carbohydrazide-2-methyl-thiophen-3-yl)-cyclopentene (0.7 g, 1.86 mmol) was dissolved in dry methanol (20 mL). To this solution were added sequentially and dropwise excess Et_3N (0.7 mL, 5 mmol) and pyridinecarboxyaldehyde (0.45 mL, 3.72 mmol), and the mixture was then stirred under reflux overnight. After this, the solution was evaporated, yielding a brown oil to which was added water 10ml and diethylether (50 mL). The resulting solution was separated and filtered, and this operation was repeated until the total dissolution of the oil. The various filtrates were mixed and washed with water and ether, yielding a light grey powder (0.85g, 83.3%). ^{1}H-NMR (400 MHZ, d_6-DMSO), δ(ppm): 11.95 (s, 2H, NHene), 8.6 (s, 2H, NH), 8.10 (m, 2H, Ar), 7.9-7.97 (m, 4H, Ar), 7.77 (s, 2H, Tph), 7.42 (m, 2H, Ar), 2.82 (t, 4H, Cp), 2.01-2.10 (m, 8H, Cp+Me). MS (ESI$^+$) m/z: 555.16 $[C_{27}H_{24}O_2N_6S_2+H]^+$.

H_2O@[$Dy_4L_4Cl_4(H_2O)_4$] (1). A solution of H_2L (20 mg, 0.036 mmol) and NaH (2.88 mg, 0.072 mmol) in pyridine (10 mL) was added to a solution of $DyCl_3{\cdot}xH_2O$ (12.21 mg, 0.036 mmol) in pyridine (10 mL). The resulting yellow solution was mixed for 2 hours, filtered and the filtrate was layered with toluene. After two days, yellow crystals were collected (15 mg, 25 % yield). Anal., found (calc% for **1**·1.5py·3H_2O): C, 45.48 (45.43); H, 3.70 (3.69); N, 10.54 (10.94); S, 7.56 (7.84). IR (KBr pellet, cm^{-1}): 3417, 2956, 2921, 2839, 1591, 1556, 1504, 1456, 1382, 1343, 1147, 1113, 1052, 865, 743, 695, 521.

H_2O@[$Tb_4L_4Cl_4(H_2O)_4$] (2). A solution of H_2L (30 mg, 0.053 mmol) and a 60% solid suspension of NaH (4.24 mg, 0.106 mmol) in pyridine (10 mL) was added to a solution of $TbCl_3{\cdot}xH_2O$ (12.71 mg, 0.034 mmol) in pyridine (10 mL). The resulting yellow solution was mixed for 2 hours, filtered and the filtrate was layered with toluene. After one day, yellow crystals were collected (31 mg, 53 % yield). Anal., found (calc% for **2**): C, 45.35 (45.26); H, 3.68 (3.47); N, 10.64 (10.92); S, 8.24 (8.33). The IR spectrum was identical to the one obtained for complex **1**.

Single Crystal X-ray Diffraction (SCXRD).

Data for compound **1** were collected at 150 K using an Oxford Diffraction Excalibur diffractometer with enhanced Mo Kα radiation (λ=0.71073 Å) at the X-ray diffraction and Fluorescence Analysis Service of the University of Zaragoza, on a yellow lath of dimensions 0.25 x 0.08 x 0.04 mm^3. Cell refinement, data reduction, and absorption corrections were performed with the CrysAlisPro suite.[57] Data for compound **2** were obtained at 100 K on a Bruker APEX II CCD diffractometer at the Advanced Light Source beam-line 11.3.1 at Lawrence Berkeley National Laboratory, from a silicon 111 monochromator (λ = 0.77490 Å), on a yellow lath of dimensions 0.40 x 0.14 x 0.10 mm^3. Data reduction and

absorption corrections were performed with SAINT and SADABS, respectively.[58] Both structures were solved by intrinsic phasing with SHELXT[59] and refined on F^2 with SHELXL.[60] In both cases, crystals appeared to damage upon removal from their mother liquor and exposure to air. Even with fast manipulation, this likely results in some areas of the cell remaining at the end of the refinement with only weak electron density peaks, that could not be modelled satisfactorily as solvent molecules. The corresponding void spaces were thus analysed and taken into account with PLATON/SQUEEZE.[61] The derived electron content/void volume are reasonable for respectively 12 and 2 additional diffuse pyridine molecules per [Ln_4], which was reflected in the formula. All details can be found in CCDC 1983839-1983840 (**1-2**) that contain the supplementary crystallographic data for this paper. These data can be obtained free of charge from The Cambridge Crystallographic Data Center via https://www.ccdc.cam.ac.uk/structures/. Crystallographic and refinement parameters are summarized in Table S1. Selected bond lengths and hydrogen bonding details are given in Tables S2 and S3.

Magnetic Properties.

Variable-temperature magnetic susceptibility data were obtained with a MPMS-XL SQUID magnetometer at the Unitat de Mesures Magnètiques of the Universitat de Barcelona. *ac* susceptibility measurements were performed with a commercial MPMS-XL SQUID magnetometer and the ACMS option of a commercial Physical Properties Measurement System (PPMS), both hosted by the Physical Measurements Unit of the Servicio General de Apoyo a la Investigación-SAI, Universidad de Zaragoza. Samples were crystals freshly recovered from their crystallization vials. To avoid orientation effects of larger crystallites, these were gently crushed and then constrained in between the two parts of the gelatin capsule used as sample holder. The data were corrected for the contribution of the capsule sample holder, determined empirically, and the sample diamagnetic contributions to the susceptibility using Pascal's constant tables. Isothermal alternating current (*ac*) data were collected with a 4 Oe field oscillating at different frequencies in the range $100 \leq \nu \leq 10.000$ Hz.

Conclusions

The newly designed ligand 1,2-bis-(5-(N'-(pyridine-2-yl-methylene)-carbohydrazide)-3-methyl-thien-3-yl)-cyclopentene (H_2L), with a photochromic dithyenylethene spacer, undergoes reversible photocyclization in solution. The flexibility of H_2L causes the folding of the tetranuclear molecular rings $H_2O@[Ln_4L_4Cl_4(H_2O)_4]$ (Ln=Tb,Dy), formed upon reaction with the corresponding $LnCl_3$ salts. The folding is driven by several intramolecular C–H···π interactions, leading to a compact tetrahedral cage. This causes the inhibition of the photochromic activity of H_2L, by forcing it to adopt its inactive conformation. The Dy cluster exhibits slow relaxation of the magnetization, enhanced under an applied magnetic field, which quenches the quantum tunnelling of the magnetization, unveiling a combination of Raman and direct mechanisms of relaxation.

Conflicts of interest

There are no conflicts to declare.

Acknowledgements

This research was supported by Spanish MINECO (CTQ2015-68370-P, PGC2018-098630-B-I00, MAT2017-86826-R, CTQ2015-64486-R), the Aragón government (E31_17R) and EU quantERA (SUMO, PCI2018-093106, PCI2018-093116), G. A. thanks the Generalitat de Catalunya for the prize ICREA Academia 2018.

Notes and references

1. K. Jinnai, R. Kabe and C. Adachi, *Chem. Commun.*, 2017, **53**, 5457-5460.
2. N. Ishikawa, M. Sugita, T. Ishikawa, S.-y. Koshihara and Y. Kaizu, *J. Am. Chem. Soc.*, 2003, **125**, 8694-8695.
3. D. N. Woodruff, R. E. P. Winpenny and R. A. Layfield, *Chem. Rev.*, 2013, **113**, 5110-5148.
4. F.-S. Guo, B. M. Day, Y.-C. Chen, M.-L. Tong, A. Mansikkamäki and R. A. Layfield, *Angew. Chem., Int. Ed.*, 2017, **56**, 11445-11449.
5. C. A. P. Goodwin, F. Ortu, D. Reta, N. F. Chilton and D. P. Mills, *Nature*, 2017, **548**, 439.
6. R. Sibille, T. Mazet, B. Malaman and M. François, *Chem., Eur. J.*, 2012, **18**, 12970-12973.
7. G. Lorusso, M. A. Palacios, G. S. Nichol, E. K. Brechin, O. Roubeau and M. Evangelisti, *Chem. Commun.*, 2012, **48**, 7592-7594.
8. M. Evangelisti, O. Roubeau, E. Palacios, A. Camón, T. N. Hooper, E. K. Brechin and J. J. Alonso, *Angew. Chem., Int. Ed.*, 2011, **50**, 6606-6609.
9. A. J. Amoroso and S. J. A. Pope, *Chem. Soc. Rev.*, 2015, **44**, 4723-4742.
10. F. Luis, A. Repolles, M. J. Martinez-Perez, D. Aguila, O. Roubeau, D. Zueco, P. J. Alonso, M. Evangelisti, A. Camon, J. Sese, L. A. Barrios and G. Aromi, *Phys. Rev. Lett.*, 2011, **107**.
11. K. S. Pedersen, A.-M. Ariciu, S. McAdams, H. Weihe, J. Bendix, F. Tuna and S. Piligkos, *J. Am. Chem. Soc.*, 2016, **138**, 5801-5804.
12. J. J. Baldovi, L. E. Rosaleny, V. Ramachandran, J. Christian, N. S. Dalal, J. M. Clemente-Juan, P. Yang, U. Kortz, A. Gaita-Arino and E. Coronado, *Inorg. Chem. Front.*, 2015, **2**, 893-897.
13. G. Aromí, F. Luis and O. Roubeau, in *Lanthanides and Actinides in Molecular Magnetism*, eds. R. A. Layfield and M. Murugesu, Wiley-WCH, 2015, pp. 185-221.
14. D. Aguilà, L. A. Barrios, V. Velasco, O. Roubeau, A. Repollés, P. J. Alonso, J. Sesé, S. J. Teat, F. Luis and G. Aromí, *J. Am. Chem. Soc.*, 2014, **136**, 14215-14222.

15. G. Aromí and O. Roubeau, in *Handbook on the Physics and Chemistry of Rare Earths*, eds. J.-C. G. Bünzli and V. K. Pecharsky, Elsevier, 2019, vol. 56, pp. 1-54.
16. F.-S. Guo, B. M. Day, Y.-C. Chen, M.-L. Tong, A. Mansikkamäki and R. A. Layfield, *Science*, 2018, **362**, 1400-1403.
17. Z. Zhu, M. Guo, X.-L. Li and J. Tang, *Coord. Chem. Rev.*, 2019, **378**, 350-364.
18. D. Pinkowicz, M. Ren, L.-M. Zheng, S. Sato, M. Hasegawa, M. Morimoto, M. Irie, B. K. Breedlove, G. Cosquer, K. Katoh and M. Yamashita, *Chem., Eur. J.*, 2014, **20**, 12502-12513.
19. M. Irie, *Chem. Rev.*, 2000, **100**, 1685-1716.
20. M. Irie, T. Fulcaminato, K. Matsuda and S. Kobatake, *Chem. Rev.*, 2014, **114**, 12174-12277.
21. Z. Y. Li, J. W. Dai, M. Damjanovic, T. Shiga, J. H. Wang, J. Zhao, H. Oshio, M. Yamashita and X. H. Bu, *Angew. Chem., Int. Ed.*, 2019, **58**, 4339-4344.
22. T. Shiga, H. Miyasaka, M. Yamashita, M. Morimoto and M. Irie, *Dalton Trans.*, 2011, **40**, 2275-2282.
23. M. Estrader, J. Salinas Uber, L. A. Barrios, J. Garcia, P. Lloyd-Williams, O. Roubeau, S. J. Teat and G. Aromí, *Angew. Chem., Int. Ed.*, 2017, **56**, 15622-15627.
24. J. Salinas-Uber, M. Estrader, J. Garcia, P. Lloyd-Williams, A. Sadurni, D. Dengler, J. van Slageren, N. F. Chilton, O. Roubeau, S. J. Teat, J. Ribas-Arino and G. Aromi, *Chem., Eur. J.*, 2017, **23**, 13648-13659.
25. M. Nihei, Y. Suzuki, N. Kimura, Y. Kera and H. Oshio, *Chem., Eur. J.*, 2013, **19**, 6946-6949.
26. M. Morimoto, H. Miyasaka, M. Yamashita and M. Irie, *J. Am. Chem. Soc.*, 2009, **131**, 9823-9835.
27. J. Salinas-Uber, L. A. Barrios, M. Estrader, O. Roubeau and G. Aromí, *Eur. J. Inorg. Chem.*, 2020, **2020**, 561-567.
28. S. Kobatake and M. Irie, *Bull. Chem. Soc. Jpn.*, 2004, **77**, 195-210.
29. D. J. van Dijken, P. Kovaříček, S. P. Ihrig and S. Hecht, *J. Am. Chem. Soc.*, 2015, **137**, 14982-14991.
30. S. Kobatake, K. Uchida, E. Tsuchida and M. Irie, *Chem. Commun.*, 2002, 2804-2805.
31. P. C. Andrews, W. J. Gee, P. C. Junk and J. G. MacLellan, *Dalton Trans.*, 2011, **40**, 12169-12179.
32. O. A. Gerasko, E. A. Mainicheva, M. I. Naumova, M. Neumaier, M. M. Kappes, S. Lebedkin, D. Fenske and V. P. Fedin, *Inorg. Chem.*, 2008, **47**, 8869-8880.
33. J.-B. Peng, Y.-P. Ren, X.-J. Kong, L.-S. Long, R.-B. Huang and L.-S. Zheng, *CrystEngComm*, 2011, **13**, 2084-2090.
34. C. Pi, L. Wan, Y. Gu, W. Zheng, L. Weng, Z. Chen and L. Wu, *Inorg. Chem.*, 2008, **47**, 9739-9741.
35. N. Kato, T. Mita, M. Kanai, B. Therrien, M. Kawano, K. Yamaguchi, H. Danjo, Y. Sei, A. Sato, S. Furusho and M. Shibasaki, *J. Am. Chem. Soc.*, 2006, **128**, 6768-6769.
36. L. Zhang, P. Zhang, L. Zhao, S.-Y. Lin, S. Xue, J. Tang and Z. Liu, *Eur. J. Inorg. Chem.*, 2013, **2013**, 1351-1357.
37. M. A. Singh-Wilmot, I. A. Kahwa, A. J. P. White, D. J. Williams and A. J. Lough, *Polyhedron*, 2010, **29**, 270-279.
38. C.-L. Liu, L.-P. Zhou, D. Tripathy and Q.-F. Sun, *Chem. Commun.*, 2017, **53**, 2459-2462.
39. J. Wang, C. He, P. Wu, J. Wang and C. Duan, *J. Am. Chem. Soc.*, 2011, **133**, 12402-12405.
40. C.-T. Yeung, K.-H. Yim, H.-Y. Wong, R. Pal, W.-S. Lo, S.-C. Yan, M. Yee-Man Wong, D. Yufit, D. E. Smiles, L. J. McCormick, S. J. Teat, D. K. Shuh, W.-T. Wong and G.-L. Law, *Nature Commun.*, 2017, **8**, 1128.
41. Y. Cui, H. L. Ngo and W. Lin, *Inorg. Chem.*, 2002, **41**, 5940-5942.
42. S.-Y. Wu, X.-Q. Guo, L.-P. Zhou and Q.-F. Sun, *Inorg. Chem.*, 2019, **58**, 7091-7098.
43. Y. Zhou, H. Li, T. Zhu, T. Gao and P. Yan, *J. Am. Chem. Soc.*, 2019, **141**, 19634-19643.
44. J. Zhang, H. Yu, C. Zhang, C. He and C. Duan, *New J. Chem.*, 2014, **38**, 3137-3145.
45. S. Zebret, C. Besnard, G. Bernardinelli and J. Hamacek, *Eur. J. Inorg. Chem.*, 2012, **2012**, 2409-2417.
46. Y. Jiao, J. Wang, P. Wu, L. Zhao, C. He, J. Zhang and C. Duan, *Chem., Eur. J.*, 2014, **20**, 2224-2231.
47. A. Vuillamy, S. Zebret, C. Besnard, V. Placide, S. Petoud and J. Hamacek, *Inorg. Chem.*, 2017, **56**, 2742-2749.
48. Y. Liu, Z. Lin, C. He, L. Zhao and C. Duan, *Dalton Trans.*, 2010, **39**, 11122-11125.
49. Q.-Q. Yan, L.-P. Zhou, H.-Y. Zhou, Z. Wang, L.-X. Cai, X.-Q. Guo, X.-Q. Sun and Q.-F. Sun, *Dalton Trans.*, 2019, **48**, 7080-7084.
50. C.-L. Liu, R.-L. Zhang, C.-S. Lin, L.-P. Zhou, L.-X. Cai, J.-T. Kong, S.-Q. Yang, K.-L. Han and Q.-F. Sun, *J. Am. Chem. Soc.*, 2017, **139**, 12474-12479.
51. Y. Liu, X. Wu, C. He, Y. Jiao and C. Duan, *Chem. Commun.*, 2009, 7554-7556.
52. J. D. Rinehart, M. Fang, W. J. Evans and J. R. Long, *J. Am. Chem. Soc.*, 2011, **133**, 14236-14239.
53. K. R. Meihaus and J. R. Long, *Dalton Trans.*, 2015, **44**, 2517-2528.
54. K. S. Pedersen, J. Dreiser, H. Weihe, R. Sibille, H. V. Johannesen, M. A. Sørensen, B. E. Nielsen, M. Sigrist, H. Mutka, S. Rols, J. Bendix and S. Piligkos, *Inorg. Chem.*, 2015, **54**, 7600-7606.
55. M. J. Giansiracusa, A. K. Kostopoulos, D. Collison, R. E. P. Winpenny and N. F. Chilton, *Chem. Commun.*, 2019.
56. S. G. McAdams, A. M. Ariciu, A. K. Kostopoulos, J. P. S. Walsh and F. Tuna, *Coord. Chem. Rev.*, 2017, **346**, 216-239.
57. , 2013, *CrysAlisPro*, Revision 5.2, Agilent Technologies, Oxfordshire. OX5 1QU, UK.
58. G. M. Sheldrick, 2012, *SAINT and SADABS*, Bruker AXS Inc., Madison, Wisconsin, USA.
59. G. Sheldrick, *Acta Cryst. A*, 2015, **71**, 3-8.
60. G. Sheldrick, *Acta Cryst. C*, 2015, **71**, 3-8.
61. A. Spek, *Acta Cryst. C*, 2015, **71**, 9-18.